Volume 10
Number 12
December 2023
Pages 5317–5986

Materials Horizons

rsc.li/materials-horizons

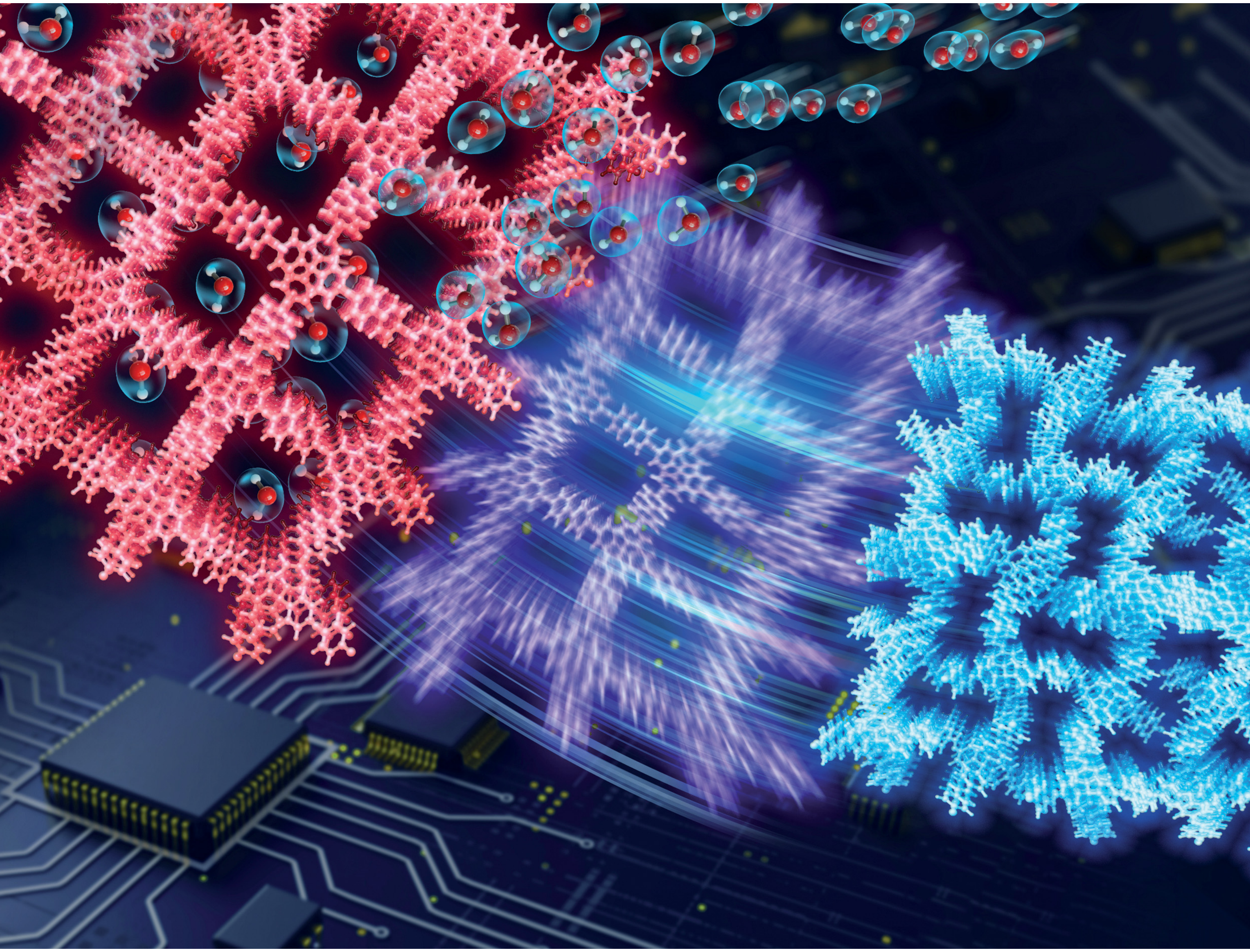

ISSN 2051-6347

ROYAL SOCIETY OF CHEMISTRY

COMMUNICATION
Sandip Thakur and Ashutosh Giri
Reversible and high-contrast thermal conductivity switching in a flexible covalent organic framework possessing negative Poisson's ratio

Materials Horizons

ROYAL SOCIETY OF CHEMISTRY

COMMUNICATION

View Article Online
View Journal | View Issue

Check for updates

Cite this: *Mater. Horiz.*, 2023, 10, 5484

Received 4th September 2023,
Accepted 4th October 2023

DOI: 10.1039/d3mh01417g

rsc.li/materials-horizons

Reversible and high-contrast thermal conductivity switching in a flexible covalent organic framework possessing negative Poisson's ratio†

Sandip Thakur and Ashutosh Giri *

The ability to dynamically and reversibly control thermal transport in solid-state systems can redefine and propel a plethora of technologies including thermal switches, diodes, and rectifiers. Current material systems, however, do not possess the swift and large changes in thermal conductivity required for such practical applications. For instance, stimuli responsive materials, that can reversibly switch between a high thermal conductivity state and a low thermal conductivity state, are mostly limited to thermal switching ratios in the range of 1.5 to 4. Here, we demonstrate reversible thermal conductivity switching with an unprecedented 18× change in thermal transport in a highly flexible covalent organic framework with revolving imine bonds. The pedal motion of the imine bonds is capable of reversible transformations of the framework from an expanded (low thermal conductivity) to a contracted (high thermal conductivity) phase, which can be triggered through external stimuli such as exposure to guest adsorption and desorption or mechanical strain. We also show that the dynamic imine linkages endow the material with a negative Poisson's ratio, thus marking a regime of materials design that combines low densities with exceptional thermal and mechanical properties.

New concepts

Reversible control of thermal conductivity in stimuli responsive materials is not only of importance from a fundamental materials science perspective but holds great promise for a plethora of applications. However, materials with fast and high-contrast thermal switching ratios for practical applications have been few and far between, thus limiting the advancements in such technologies. We demonstrate an unprecedented 18× change in thermal conductivity in a highly flexible covalent organic framework endowed with swift and reversible thermal transport control that exceeds the thermal switching ratios reported thus far in any material system. Through systematic atomistic simulations, we show that the key mechanism dictating such large changes in the intrinsic thermal transport properties is the dynamic pedal motion of the imine bonds that allows for the reversible transitions of the flexible covalent organic framework from expanded, low thermal conductivity to contracted, high thermal conductivity states. Furthermore, we also show that these lightweight materials are endowed with highly flexible frameworks and a negative Poisson's ratio, thus combining a host of superlative physical properties in one material system.

Actively manipulating the thermal conductivity of materials can not only enable novel directions of research in fundamental science but can also have transformative impacts on various technologies through proper engineering of new thermal diodes, regulators and switches.[1] For example, materials with dynamic and high thermal conductivity switching ratios can transform the field of nanophononics,[2,3] revolutionize thermal management strategies for microelectronics,[4,5] lead to the emergence of thermally driven logic gates and transistors,[1,2] and provide advancements in all solid-state electrocaloric refrigeration.[6] Although the efficiencies of such devices cannot rival their well-established electrical analogs that modulate current flow, the prospect of utilizing wasted heat as the source to 'power' such thermally driven devices is very appealing with far-reaching consequences, such as that of combating the issue of the ever-depleting nonrenewable energy resources. Yet, the advancements in such technologies are critically hinged upon designing materials with reversible and high-contrast thermal switching capabilities with efficient toggling between "on-state" (high thermal conductivity) and "off-state" (low thermal conductivity), which has been extremely difficult to realize in materials.

In the last two decades, there have been several material systems that have demonstrated the thermal switching phenomena triggered by various external stimuli (Fig. 1). These most notably include: changes in molecular orientation in

---

Department of Mechanical, Industrial and Systems Engineering, University of Rhode Island, Kingston, RI 02881, USA. E-mail: ashgiri@uri.edu

† Electronic supplementary information (ESI) available: References for Fig. 1 and Fig. 4b, details of the equilibrium molecular dynamics (EMD) and nonequilibrium molecular dynamics (NEMD) simulations, calculations of radial distribution functions, X-ray diffraction patterns, stress–strain calculations on COF-300, vibrational density of states calculations, and videos of pore expansion and contraction facilitating the low and high thermal conductivity states, respectively. See DOI: https://doi.org/10.1039/d3mh01417g

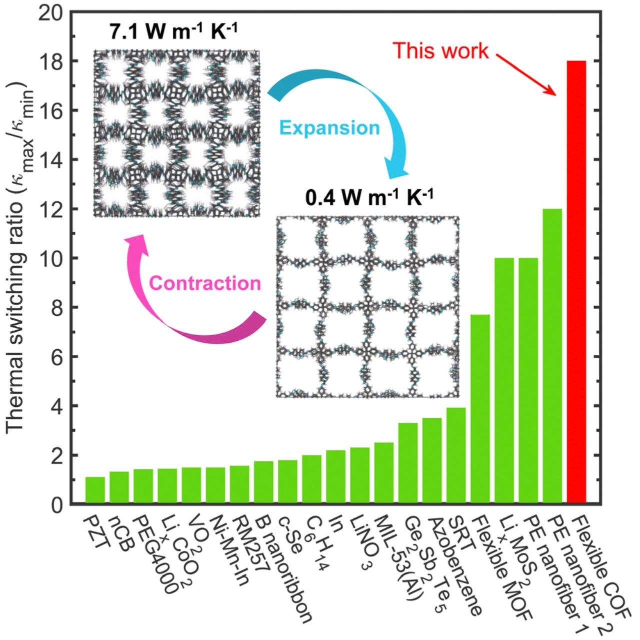

Fig. 1 Thermal switching ratios ($\kappa_{max}/\kappa_{min}$, where κ_{min} is the minimum and κ_{max} is the maximum thermal conductivity) for various types of materials studied in prior literature. The thermal conductivity switching ratios for most material systems range from 1.5 to 4. The flexible 3D COF studied in this work demonstrates an unprecedented 18× change in thermal transport. This is facilitated by the reversible transitions between expansion (low thermal conductivity state) and contraction (high thermal conductivity state) of the flexible COF in response to external stimuli.

liquid crystal networks from an externally applied magnetic field to increase their thermal conductivity from $\sim$0.2 W m^{-1} K^{-1} to $\sim$0.35 W m^{-1} K^{-1},[7] electric field induced changes in the nanoscale ferroelastic domains resulting in an 11% increase in thermal conductivity in lead zirconate titanate thin films,[8] light triggered increase of $\sim$3× in thermal conductivity of azobenzene polymers,[9] reversible delithiation in lithium cobalt oxide with a switching ratio of $\sim$3,[10] and wetting of tandem repeat proteins of squid ring teeth-based bio-polymers to achieve a swift 4× change in thermal conductivity.[11] However, the largest thermal switching ratio for any solid–solid or solid–liquid phase transition has been measured in crystalline polyethylene nanofibers with structural phase transition, where a $\sim$10× change in thermal transport was obtained *via* electrical heating.[12] Similarly, the largest tunability in heat conduction has been calculated for polyethylene nanofibers by inducing phase transitions through strain effects with a 12× change in thermal conductivity.[13] Taken together, it is clear that reversible structural transitions in polymeric materials induced through some external stimuli present a facile platform to achieving the highly sought-after thermal switching phenomena with large differences in the "on" and "off" states. Here, we demonstrate an unprecedented $\sim$18× change in reversible thermal conductivity (as highlighted in Fig. 1) for a flexible three-dimensional (3D) covalent organic framework (COF). We show that the dynamic motion of imine linkages controllable *via* external triggers (such as through guest adsorption and desorption, for example)[14] allows variations of the "free-volume" space in the COF, whereby the open pores can expand (upon adsorption) or contract (upon desorption), thus providing an efficient mechanism for high-contrast thermal conductivity switching.

With high porosities, extended periodicities, and large surface areas, COFs have emerged as new frontier materials that combine unique physical properties arising mostly from their highly modular architectures.[15–22] This combination of superlative physical properties positions COFs as attractive candidates for a plethora of applications over conventional polymers or even their metal organic framework (MOF) cousins.[15] For instance, COFs (when compared to MOFs) have shown a better promise for several thermal management applications,[23] owing to their relatively higher thermal conductivities originating from their extended crystalline frameworks comprising of strongly bonded light atoms (*e.g.*, C, N, O, and B).[18,19,24–26] In contrast, MOFs typically have lower thermal conductivities (in the range of $\sim$0.3 to 1 W m^{-1} K^{-1}),[27–41] since vibrational scattering is greatly facilitated by their large atomic mass mismatches between the heavy metal nodes and the light organic linkers. Recently, however, atomistic simulations have shown that 'breathing' MOFs can possess reversible thermal conductivities resulting from phase transitions.[38,42,43] In this regard, COFs should provide a better platform for achieving reversible and higher contrast thermal conductivity switching based on their superior thermal performance and unique chemical makeups.

In this work, we use reactive molecular dynamics (MD) simulations to demonstrate a room temperature thermal conductivity switching ratio of 18× in a 3D COF composed of dynamic imine linkages. The thermal conductivity can be modulated across a wide range through external stimuli capable of toggling between the expanded phases possessing thermal conductivities as low as 0.4 W m^{-1} K^{-1} and contracted (yet, 'stress-free') phases possessing high thermal conductivities as much as 7.1 W m^{-1} K^{-1} (as schematically shown in the inset of Fig. 1). We attribute the enhancement in thermal conductivity to two factors, namely, the better alignment of the polymeric chains along the direction of heat conduction and the reduction of vibrational scattering at the pore walls due to reduced porosities. Along with the exceptional thermal conductivity switching, we also show that these materials combine unique mechanical properties such as being highly flexible and possessing negative Poisson's ratio, a combination of physical properties that are unique to these stimuli-responsive COFs.

We base our calculations on a flexible 3D COF recently synthesized *via* imine condensation of (3,3′-bipyridine)-6,6′-dicarbaldehyde and tetra(4-anilyl)methane to form 1D channels,[14] as shown in Fig. 2. The 1D pore channels are similar to that of the prototypical COF-300 structure (see Fig. S4, ESI†). However, the key feature that separates these COFs, and also enables thermal conductivity switching in the flexible COF, is the revolving nature of its' imine linkers, which act as molecular pedals[44] facilitating the transition of the framework from a contracted phase to an expanded phase, as shown in Fig. 2. Whereas, rigid

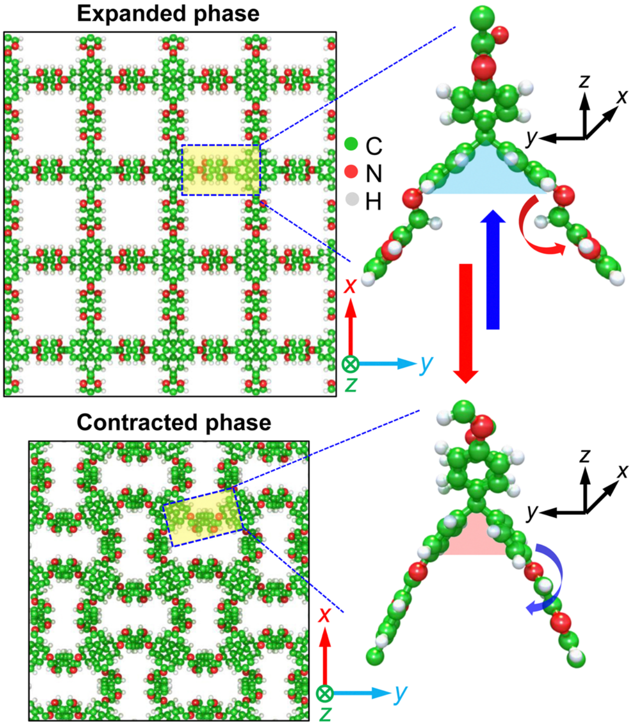

Fig. 2 Schematics of our flexible COF structures with the expanded and contracted frameworks. Since the *x*- and *y*-directions are identical, we denote it as the in-plane direction and the *z*-direction as the cross-plane direction for our discussions. The magnified views of the imine linkages demonstrating the pedal-like motion around the imine bond are also shown. The dynamic motion of these bonds facilitates the expansion and contraction of the framework as highlighted by the angle between the linkages that varies with the pedal motion, thus changing the 'free-volume' space available.

imine-linked COFs (such as COF-300) do not possess such stretchable pore geometries capable of reversible pore expansion/contraction as stimuli responses, for example, to gas adsorption/desorption. Such a stimuli responsiveness unique to the dynamic nature of the flexible COF framework can be exploited for thermal conductivity switching applications as we discuss in detail below. Note that since the imine linkages are identical in the *x*- and *y*-directions, we prescribe these principle directions as the in-plane direction and the *z*-direction as the cross-plane direction in our discussions below.

All our simulations are conducted with the large atomic molecular massively parallel simulator (LAMMPS) package[45] and the details of our calculations and analyses can be found in the ESI.† For our simulations, we use the reactive potential, ReaxFF,[46] to describe the interatomic interactions that takes into account the distance-dependent bond order function capable of accounting for the dynamic and responsive nature of the flexible COF framework. Note, the interatomic potential is successful in replicating the experimental structure of the expanded and contracted phases of the flexible COF as evident from our calculations revealing the structural characteristics such as the X-ray diffraction patterns (Fig. S4–S6, ESI†).

Fig. 3a shows the calculated room temperature thermal conductivities of the flexible COF as a function of the unit cell volume. Along with the high-contrast in the thermal conductivity of the expanded and contracted phases, another noteworthy aspect in Fig. 3a is the increase in anisotropy of thermal conductivity as the dynamic framework transitions to a more contracted phase. More specifically, it is interesting to note that the cross-plane thermal conductivity can be increased by as much as 18× upon contraction, while the in-plane thermal conductivity demonstrates a comparatively small increase when the framework transitions from an expanded to a contracted phase and *vice versa*. The origin of such anisotropic response is partly rooted in the variation of chain alignment along the direction of heat conduction. For the cross-plane direction, as the framework transitions to a more contracted phase, the polymeric chains align better along that direction, thus enhancing the efficacy of heat transfer in that direction. This is quantitatively shown in Fig. 3b where we plot the cross-plane thermal conductivity as a function of the angle between the linker and the in-plane direction. As the structure transitions from the expanded phase to the contracted phase, the polymer chains align better in the cross-plane direction (Fig. 3c and d), thus facilitating heat flow in that direction. In contrast, for the in-plane direction, the chain alignment is disrupted upon contraction (see Fig. 2), which should result in a lower heat conduction along that direction due to chain misalignment. However, the decrease in pore sizes with contraction leads to the decrease in vibrational scattering at the pore walls, thus counteracting the effect of chain alignment to the heat conduction along the in-plane direction.

For comparison, we also calculate the thermal conductivity of COF-300, which has rigid imine linkages comprising the 3D framework, as a function of the unit cell volume in Fig. 4a. The change in thermal conductivity of the rigid COF-300 shows a completely different response to variations in the porosity induced *via* external strain, whereby the thermal conductivity is higher in both the in-plane and cross-plane directions with the increase in the pore volume. Although there is this stark difference between the flexible and the rigid COFs, the common trait between the two structures, in terms of heat conduction, is the fact that the enhancement in thermal conductivity for both the structures can be ascribed to better chain alignment along the heat conduction direction; for COF-300, chains align better in the direction of heat flow resulting from the response to the hydrostatic tension applied to the computational domain (inset of Fig. 4a), whereas the contracted phase of the flexible COF leads to better alignment of the imine linkers along the cross-plane direction (Fig. 3c). Altogether, this comparison of the thermal conductivity response to pore contraction/expansion of the rigid *versus* the flexible frameworks highlights the importance of the revolving nature of the imine bonds as molecular pedals in dictating the thermal switching response of the flexible COF.

The result for COF-300 is counterintuitive to conventional materials where higher densities generally are associated with higher thermal conductivities; while aerogels and porous framework materials have relatively lower thermal conductivities, fully dense semiconductors such as diamond and cubic boron

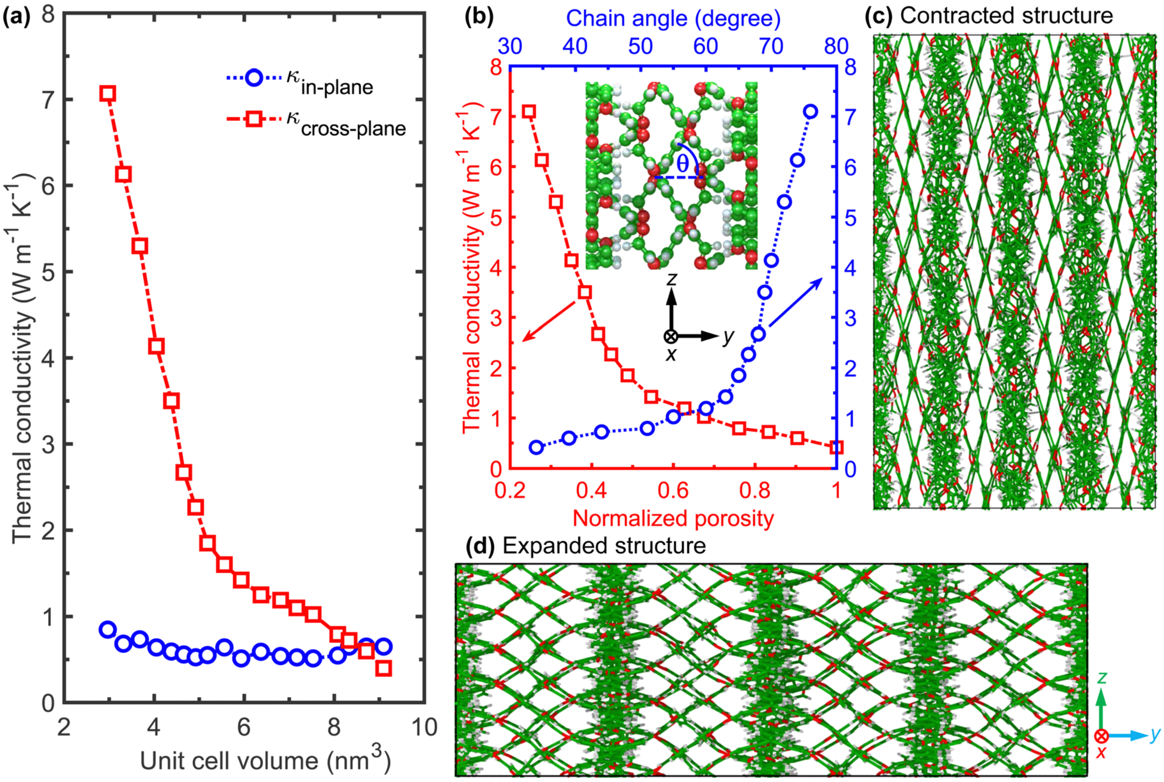

Fig. 3 (a) Thermal conductivity as a function of unit cell volume for our flexible COF showing the monotonic decrease of the cross-plane thermal conductivity with increasing volume (or porosity). For the in-plane direction, the thermal conductivity has negligible change as porosity or unit cell volume increases. (b) As the framework expands and the porosity increases, the angle between the polymer chains and the in-plane direction decreases. (c) The cross-plane (*z*-direction) thermal conductivity increases with contraction since the polymeric chains are better aligned along that direction. (d) In contrast, it decreases for the expanded structure since the polymeric chains are better aligned along the in-plane direction. The increase in porosity with expansion counteracts the influence of chain alignment in the in-plane direction, thus leading to a negligible change in the in-plane thermal conductivity with unit cell volume as shown in (a).

nitride have much higher thermal conductivities (Fig. 4b). This fact, taken together with the results discussed above, suggests that chain alignment is the predominant factor controlling the thermal conductivity for COFs, and as such, can provide guidance for designing COFs with high thermal conductivities for thermal management applications. Moreover, although the densities of the rigid and flexible COFs are comparable to the densities of aerogels, their thermal conductivities, especially for the contracted phase of our flexible COF, are more than an order of magnitude greater (for most cases) than aerogels or other porous materials with similar densities (see Fig. 4b). Therefore, along with the remarkable thermal conductivity switching response for the flexible COFs, our results also mark a new regime of materials design combining ultralow densities with relatively high thermal conductivities, which could be highly beneficial for the design of ultralight-weight structural materials.[49,50]

It is worth noting that the experimentally observed reversible crystal transformation of the flexible COF was through guest adsorption and desorption.[14] In the case of adsorption, the thermal conductivity of the COF might be influenced through scattering of the framework phonons by the guest species, as has been recently shown experimentally for MOFs with various adsorbed guest molecules.[30,36] Such a guest-induced scattering leads to even lower thermal conductivities as compared to the thermal conductivities calculated for our expanded (empty) frameworks, thus potentially increasing the magnitude of the switching ratio calculated in this work. However, we caution that variations in the guest species and their diffusivities could have varying effects on the overall thermal conductivities of the guest-infiltrated frameworks providing a potentially additional knob to tune their thermal transport properties.[24,25,33] Furthermore, in view of host–guest interactions, recently it has also been shown that the thermal conductivity of organic framework materials can be enhanced significantly *via* increasing the level of interpenetration.[47,48,51,52] For instance, our recent study demonstrated that a 3-fold interpenetration can lead to as much as a 6-fold increase in the room temperature thermal conductivity of COF-300.[47] This enhancement in the heat conduction efficacy was attributed to increased phonon hardening, reduced vibrational scattering at the pores, and lattice stiffening resulting from the supramolecular interactions between the individual frameworks. It should also be noted that along with documentation of several recent advancements in COFs that are responsive to several different external stimuli such as pH levels, metal ions, electricity, light and many others,[53]

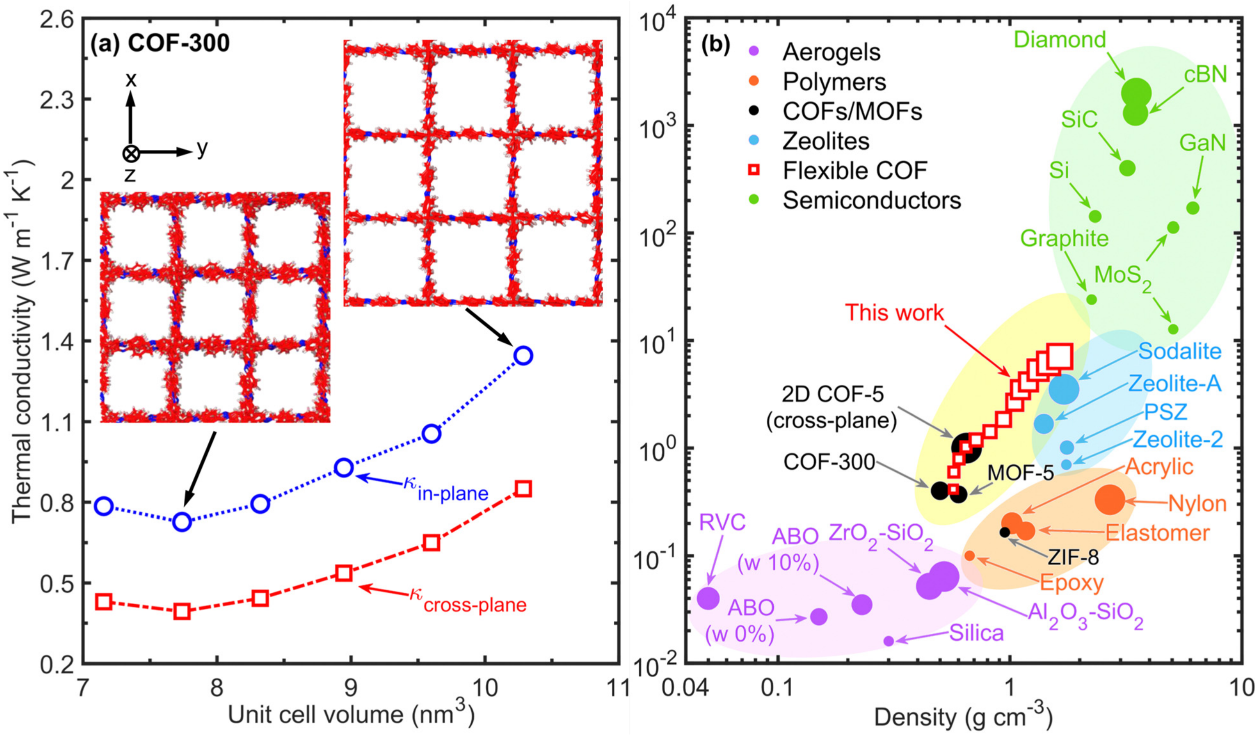

Fig. 4 (a) Thermal conductivity as a function of unit cell volume for our COF-300 framework. In contrast to our flexible COF, expansion of the framework leads to a higher thermal conductivity in COF-300 due to better chain alignment along the principal directions (as shown in the inset). (b) Comparison of thermal conductivity at room temperature as a function of density for our flexible COF with common aerogels, polymers, zeolites, and semiconductors. In general, higher densities are associated with higher thermal conductivities. However, the flexible COFs span a regime of materials design combining low densities with relatively higher thermal conductivity, which has been critically missing. Moreover, our flexible COF also possesses higher thermal conductivities as compared to other framework materials such as COF-300,[47] MOF-5,[28,48] and a recent measurement of cross-plane thermal conductivity of 2D COF-5.[19]

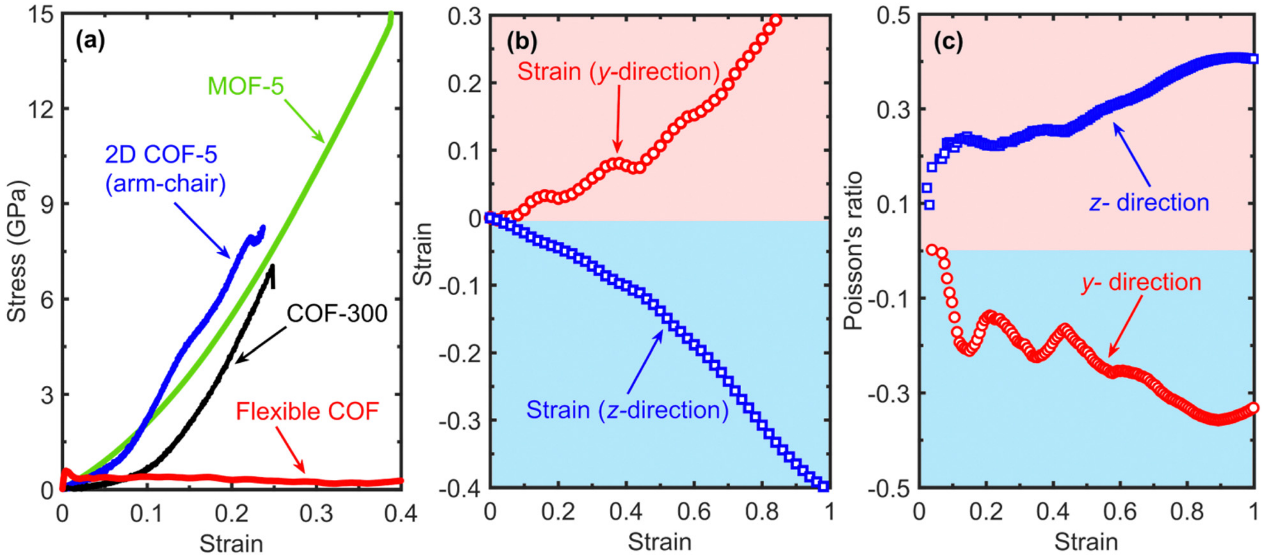

Fig. 5 (a) Comparison of stress *versus* strain curves calculated from uniaxial tension applied in the *x*-direction for our flexible COF along with the results for COF-300, MOF-5 and 2D COF-5 (from our prior work).[18] Although the strain causes stress buildup for the other porous frameworks, our flexible COF shows negligible stress even upon strain levels of 80%, which highlights its' highly flexible nature. (b) The resultant strain in the *z*- and *y*-directions *versus* the applied uniaxial strain in the *x*-direction. While the flexible COF domain contracts in the *z*-direction, the domain expands considerably in the *y*-direction. (c) The Poisson's ratio extracted from our uniaxial tensile simulations showing the nonlinear negative values for the *y*-direction as a function of strain in the *x*-direction where tension is applied.

the guest-induced structural changes in COFs has most notably been shown to be very swift with response times below 200 ms.[54] Therefore, COFs hold great promise for not only high-contrast but also fast reversible thermal conductivity switching applications.

Finally, we reveal the ultraflexible nature of our dynamic COF by monitoring the stress response to uniaxial tension of the contracted phase along the in-plane direction, as shown in Fig. 5a. For comparison, we also show the stress–strain responses of other similar porous frameworks, namely, COF-300, MOF-5 and 2D COF-5 (taken from our prior work)[18] under uniaxial tension. While there is minimal stress build-up for our dynamic COF, considerable increases in stresses are observed for the rest of the structures. This again highlights the role of the molecular pedal motion of the imine bonds for facile switching between the contracted and expanded phases in response to external stimuli, such as strain in this case. However, guest absorption/desorption can also lead to similar phase changes for 'stress-free' structures.[14]

Our uniaxial tensile simulations on the dynamic COF also reveal a unique physical attribute in these COFs, namely, a negative Poisson's ratio when uniaxial strain is applied along the in-plane direction. As shown in Fig. 5b, while the length of the computational domain shrinks in the cross-plane direction (represented by the negative strain), the computational domain expands along the *y*-direction when uniaxial strain is applied along the *x*-direction. The resulting Poisson's ratios in the cross-plane and the in-plane directions due to uniaxial tensile deformation are shown in Fig. 5c. The mechanism dictating the negative Poisson's ratio along the in-plane direction also derives from the same pedal motion of the imine linkers that facilitates thermal conductivity switching, which is absent in the rigid COF-300 structure for which a positive Poisson's ratio is calculated in all directions (Fig. S9 and S10, ESI†). This auxeticity that we observe for our flexible COF is a unique result since most materials shrink laterally when stretched along the orthogonal direction, characterizing a positive Poisson's ratio with a typical value of 0.33 for most materials.[55]

Materials with a negative Poisson's ratio, although rare, can counterintuitively expand laterally in response to an orthogonal tensile force,[56–62] and are usually accompanied by anomalous or enhanced physical properties,[18,63–68] as with the case of our flexible COF. As such, these materials can not only be transformative for thermally-driven applications, but can also find widespread applications in fields ranging from tissue engineering, and medicine to aerospace and defence.[69–72] In this respect, although auxetic behavior has been previously observed for other materials, such as in some two-dimensional materials,[73–75] honeycomb structures,[65,76] molecular structures,[18,58–60,77,78] and metal organic frameworks,[79,80] the flexible COFs studied in this work combine ultra-flexibility and negative Poisson's ratio with low densities and tunable thermal conductivities, a combination of material properties that highlights a new frontier in the design of multifunctional materials.

In summary, we have demonstrated an unprecedented room-temperature thermal conductivity switching ratio of 18 in a flexible 3D COF capable of reversibly transitioning from an expanded, low thermal conductivity state, to a contracted, high thermal conductivity state. Our reactive MD simulations have revealed that chain alignment, a critical factor in dictating heat transport in these materials, can be leveraged to modulate the reversible thermal conductivity of the dynamic COF. The key to achieving this dynamic modulation and the high-contrast thermal switching relies on the molecular pedal motion of the imine bonds that respond to exposure from an external stimuli such as mechanical strain or guest adsorption/desorption. Along with their exceptional thermal properties, we have also shown that these COFs are highly flexible and possess negative Poisson's ratio, thus marking a new regime for designing multifunctional materials combining a host of superior physical attributes.

Conflicts of interest

There are no conflicts to declare.

Acknowledgements

This work is supported by the Office of Naval Research, Grant No. N00014-21-1-2622. Acknowledgement is made to the donors of the American Chemical Society Petroleum Research Fund for partial support of this research. The work is also partially supported by the National Science Foundation (NSF Award No. 2119365).

References

1 G. Wehmeyer, T. Yabuki, C. Monachon, J. Wu and C. Dames, *Appl. Phys. Rev.*, 2017, **4**, 041304.
2 N. Li, J. Ren, L. Wang, G. Zhang, P. Hänggi and B. Li, *Rev. Mod. Phys.*, 2012, **84**, 1045.
3 M. Nomura, R. Anufriev, Z. Zhang, J. Maire, Y. Guo, R. Yanagisawa and S. Volz, *Mater. Today Phys.*, 2022, **22**, 100613.
4 T. Du, Z. Xiong, L. Delgado, W. Liao, J. Peoples, R. Kantharaj, P. R. Chowdhury, A. Marconnet and X. Ruan, *Nat. Commun.*, 2021, **12**, 4915.
5 A. L. Moore and L. Shi, *Mater. Today*, 2014, **17**, 163–174.
6 A. Mischenko, Q. Zhang, J. Scott, R. Whatmore and N. Mathur, *Science*, 2006, **311**, 1270–1271.
7 J. Shin, M. Kang, T. Tsai, C. Leal, P. V. Braun and D. G. Cahill, *ACS Macro Lett.*, 2016, **5**, 955–960.
8 J. F. Ihlefeld, B. M. Foley, D. A. Scrymgeour, J. R. Michael, B. B. McKenzie, D. L. Medlin, M. Wallace, S. Trolier-McKinstry and P. E. Hopkins, *Nano Lett.*, 2015, **15**, 1791–1795.
9 J. Shin, J. Sung, M. Kang, X. Xie, B. Lee, K. M. Lee, T. J. White, C. Leal, N. R. Sottos and P. V. Braun, *et al.*, *Proc. Natl. Acad. Sci. U. S. A.*, 2019, **116**, 5973–5978.
10 J. Cho, M. D. Losego, H. G. Zhang, H. Kim, J. Zuo, I. Petrov, D. G. Cahill and P. V. Braun, *Nat. Commun.*, 2014, **5**, 4035.

11 J. A. Tomko, A. Pena-Francesch, H. Jung, M. Tyagi, B. D. Allen, M. C. Demirel and P. E. Hopkins, *Nat. Nanotechnol.*, 2018, **13**, 959–964.

12 R. Shrestha, Y. Luan, S. Shin, T. Zhang, X. Luo, J. S. Lundh, W. Gong, M. R. Bockstaller, S. Choi and T. Luo, *et al.*, *Sci. Adv.*, 2019, **5**, eaax3777.

13 T. Zhang and T. Luo, *ACS Nano*, 2013, **7**, 7592–7600.

14 Y.-X. Ma, Z.-J. Li, L. Wei, S.-Y. Ding, Y.-B. Zhang and W. Wang, *J. Am. Chem. Soc.*, 2017, **139**, 4995–4998.

15 R. P. Bisbey and W. R. Dichtel, *ACS Cent. Sci.*, 2017, **3**, 533–543.

16 P. J. Waller, S. J. Lyle, T. M. Osborn Popp, C. S. Diercks, J. A. Reimer and O. M. Yaghi, *J. Am. Chem. Soc.*, 2016, **138**, 15519–15522.

17 A. P. Cote, A. I. Benin, N. W. Ockwig, M. O'Keeffe, A. J. Matzger and O. M. Yaghi, *Science*, 2005, **310**, 1166–1170.

18 A. Giri, A. M. Evans, M. A. Rahman, A. J. McGaughey and P. E. Hopkins, *ACS Nano*, 2022, **16**, 2843–2851.

19 A. M. Evans, A. Giri, V. K. Sangwan, S. Xun, M. Bartnof, C. G. Torres-Castanedo, H. B. Balch, M. S. Rahn, N. P. Bradshaw and E. Vitaku, *et al.*, *Nat. Mater.*, 2021, **20**, 1142–1148.

20 F. Kang, Y. Lin, S. Zhang, Z. Tan, X. Wang, J. Yang, Y.-K. Peng, W. Zhang, C.-S. Lee and W. Huang, *et al.*, *ACS Appl. Mater. Interfaces*, 2023, **15**, 9431–9438.

21 Y. Shi, J. Yang, F. Gao and Q. Zhang, *ACS Nano*, 2023, **17**, 1879–1905.

22 F. Kang, X. Wang, C. Chen, C.-S. Lee, Y. Han and Q. Zhang, *J. Am. Chem. Soc.*, 2023, **145**, 15465–15472.

23 J. Kwon, H. Ma, A. Giri, P. E. Hopkins, N. B. Shustova and Z. Tian, *ACS Nano*, 2023, **17**, 15222–15230.

24 A. Giri and P. E. Hopkins, *Nano Lett.*, 2021, **21**, 6188–6193.

25 M. A. Rahman, C. J. Dionne and A. Giri, *ACS Appl. Mater. Interfaces*, 2022, **14**, 21687–21695.

26 M. A. Rahman, C. J. Dionne and A. Giri, *Nano Lett.*, 2022, **22**, 8534–8540.

27 M. Islamov, P. Boone, H. Babaei, A. J. McGaughey and C. E. Wilmer, *Chem. Sci.*, 2023, **14**, 6592–6600.

28 B. Huang, Z. Ni, A. Millward, A. McGaughey, C. Uher, M. Kaviany and O. Yaghi, *Int. J. Heat Mass Transfer*, 2007, **50**, 405–411.

29 X. Zhang and J. Jiang, *J. Phys. Chem. C*, 2013, **117**, 18441–18447.

30 H. Babaei, M. E. DeCoster, M. Jeong, Z. M. Hassan, T. Islamoglu, H. Baumgart, A. J. McGaughey, E. Redel, O. K. Farha and P. E. Hopkins, *et al.*, *Nat. Commun.*, 2020, **11**, 4010.

31 H. Babaei, A. J. McGaughey and C. E. Wilmer, *Chem. Sci.*, 2017, **8**, 583–589.

32 H. Babaei and C. E. Wilmer, *Phys. Rev. Lett.*, 2016, **116**, 025902.

33 L. Han, M. Budge and P. A. Greaney, *Comput. Mater. Sci.*, 2014, **94**, 292–297.

34 J. Wieme, S. Vandenbrande, A. Lamaire, V. Kapil, L. Vanduyfhuys and V. Van Speybroeck, *ACS Appl. Mater. Interfaces*, 2019, **11**, 38697–38707.

35 H. Babaei, A. J. McGaughey and C. E. Wilmer, *ACS Appl. Mater. Interfaces*, 2018, **10**, 2400–2406.

36 M. E. DeCoster, H. Babaei, S. S. Jung, Z. M. Hassan, J. T. Gaskins, A. Giri, E. M. Tiernan, J. A. Tomko, H. Baumgart and P. M. Norris, *et al.*, *J. Am. Chem. Soc.*, 2022, **144**, 3603–3613.

37 K. J. Erickson, F. Léonard, V. Stavila, M. E. Foster, C. D. Spataru, R. E. Jones, B. M. Foley, P. E. Hopkins, M. D. Allendorf and A. A. Talin, *Adv. Mater.*, 2015, **27**, 3453–3459.

38 A. Lamaire, J. Wieme, A. E. Hoffman and V. Van Speybroeck, *Faraday Discuss.*, 2021, **225**, 301–323.

39 S. Zhang, J. Liu and L. Liu, *RSC Adv.*, 2021, **11**, 36928–36933.

40 B. Cui, C. O. Audu, Y. Liao, S. T. Nguyen, O. K. Farha, J. T. Hupp and M. Grayson, *ACS Appl. Mater. Interfaces*, 2017, **9**, 28139–28143.

41 B. Huang, A. McGaughey and M. Kaviany, *Int. J. Heat Mass Transfer*, 2007, **50**, 393–404.

42 H. Babaei, K. R. Meihaus and J. R. Long, *Chem. Mater.*, 2023, **35**, 6220–6226.

43 K. B. Sezginel, S. Lee, H. Babaei and C. E. Wilmer, *J. Phys. Chem. C*, 2020, **124**, 18604–18608.

44 J. Harada and K. Ogawa, *Chem. Soc. Rev.*, 2009, **38**, 2244–2252.

45 S. Plimpton, *J. Comput. Phys.*, 1995, **117**, 1–19.

46 A. C. Van Duin, S. Dasgupta, F. Lorant and W. A. Goddard, *J. Phys. Chem. A*, 2001, **105**, 9396–9409.

47 S. Thakur and A. Giri, *J. Mater. Chem. A*, 2023, **11**, 18660–18667.

48 K. B. Sezginel, P. A. Asinger, H. Babaei and C. E. Wilmer, *Chem. Mater.*, 2018, **30**, 2281–2286.

49 L. R. Meza, S. Das and J. R. Greer, *Science*, 2014, **345**, 1322–1326.

50 A. Giri, J. Tomko, J. T. Gaskins and P. E. Hopkins, *Nanoscale*, 2018, **10**, 22166–22172.

51 T. Ma, J. Li, J. Niu, L. Zhang, A. S. Etman, C. Lin, D. Shi, P. Chen, L.-H. Li and X. Du, *et al.*, *J. Am. Chem. Soc.*, 2018, **140**, 6763–6766.

52 C. J. Dionne, M. A. Rahman, P. E. Hopkins and A. Giri, *Nano Lett.*, 2022, **22**, 3071–3076.

53 P. She, Y. Qin, X. Wang and Q. Zhang, *Adv. Mater.*, 2022, **34**, 2101175.

54 L. Ascherl, E. W. Evans, M. Hennemann, D. Di Nuzzo, A. G. Hufnagel, M. Beetz, R. H. Friend, T. Clark, T. Bein and F. Auras, *Nat. Commun.*, 2018, **9**, 3802.

55 G. N. Greaves, A. L. Greer, R. S. Lakes and T. Rouxel, *Nat. Mater.*, 2011, **10**, 823–837.

56 E. Kittinger, J. Tichy and E. Bertagnolli, *Phys. Rev. Lett.*, 1981, **47**, 712.

57 K. E. Evans, M. Nkansah, I. Hutchinson and S. Rogers, *Nature*, 1991, **353**, 124.

58 K. E. Evans, A. Alderson and F. R. Christian, *J. Chem. Soc., Faraday Trans.*, 1995, **91**, 2671–2680.

59 J. N. Grima, R. Jackson, A. Alderson and K. E. Evans, *Adv. Mater.*, 2000, **12**, 1912–1918.

60 N. Pour, L. Itzhaki, B. Hoz, E. Altus, H. Basch and S. Hoz, *Angew. Chem.*, 2006, **118**, 6127–6129.

61 J.-W. Jiang, S. Y. Kim and H. S. Park, *Appl. Phys. Rev.*, 2016, **3**, 041101.

62 C. Huang and L. Chen, *Adv. Mater.*, 2016, **28**, 8079–8096.

63 A. Yeganeh-Haeri, D. J. Weidner and J. B. Parise, *Science*, 1992, **257**, 650–652.

64 K. Alderson, A. Pickles, P. Neale and K. Evans, *Acta Metall. Mater.*, 1994, **42**, 2261–2266.

65 R. Lakes, *Science*, 1987, **235**, 1038–1040.

66 N. R. Keskar and J. R. Chelikowsky, *Nature*, 1992, **358**, 222–224.

67 R. H. Baughman, J. M. Shacklette, A. A. Zakhidov and S. Stafström, *Nature*, 1998, **392**, 362–365.

68 L. J. Hall, V. R. Coluci, D. S. Galvão, M. E. Kozlov, M. Zhang, S. O. Dantas and R. H. Baughman, *Science*, 2008, **320**, 504–507.

69 P. Mardling, A. Alderson, N. Jordan-Mahy and C. L. Le Maitre, *Biomater. Sci.*, 2020, **8**, 2074–2083.

70 Y. J. Park and J. K. Kim, *et al.*, *Adv. Mater. Sci. Eng.*, 2013, **2013**, 853289.

71 K. E. Evans and A. Alderson, *Adv. Mater.*, 2000, **12**, 617–628.

72 L. Rothenburg, A. Ai Berlin and R. J. Bathurst, *Nature*, 1991, **354**, 470–472.

73 G. Qin and Z. Qin, *npj Comput. Mater.*, 2020, **6**, 51.

74 J.-W. Jiang and H. S. Park, *Nat. Commun.*, 2014, **5**, 4727.

75 J.-W. Jiang, T. Chang, X. Guo and H. S. Park, *Nano Lett.*, 2016, **16**, 5286–5290.

76 M. F. Ashby and L. J. Gibson, *Press Syndicate of the University of Cambridge*, *Cambridge*, UK, 1997, 175–231.

77 C. He, P. Liu and A. C. Griffin, *Macromolecules*, 1998, **31**, 3145.

78 R. H. Baughman and D. S. Galvao, *Nature*, 1993, **365**, 735–737.

79 E. Jin, I. S. Lee, D. Kim, H. Lee, W.-D. Jang, M. S. Lah, S. K. Min and W. Choe, *Sci. Adv.*, 2019, **5**, eaav4119.

80 M. R. Ryder, B. Civalleri, G. Cinque and J.-C. Tan, *CrystEngComm*, 2016, **18**, 4303–4312.